central load ($p_2 = 0$) is depicted in Fig. 2 and the interaction curves are symmetric about the ray $p_1 = p_3$. Finally, symmetric load distributions are considered in Fig. 3 where p_1 and p_3 are equal to each other and their ratio with p_2 is varied.

As one might expect, the interaction curves move closer to the origin with increasing pulse duration t_f. In other words, the critical value of the initial load magnitude at $t = 0$ decreases if the load is applied to the arch for a longer time. Step loading provides the limiting case. (If one were to use the pulse areas $p_k t_f/2$ as the coordinates on the axes, the interaction curves would move inward with decreasing pulse duration and would approach the curve for impulse loads.) The presence of damping is seen to increase the critical loads, except in the case of step loading in Fig. 3, and to cause little change in the shapes of the curves, except in the aforementioned case and for $t_f = \frac{1}{8}$ in Fig. 2 near the ray $p_1 = p_3$.

The lowest critical load, as far as the sum of the magnitudes is concerned, occurs when either p_1 or p_3 is applied by itself. The arch is especially resistant to snap-through when the loading is symmetric. At $p_1 = p_3$ in Fig. 2, the interaction curves develop a spike as $t_f \to 0$, indicating extreme sensitivity to asymmetric imperfections.

Knowledge of the shapes of interaction curves can sometimes be used to obtain bounds and approximations for critical load combinations in related problems. In most of the results presented here, for example, a straight line connecting the critical loads on the two axes furnishes stable load combinations (although they are sometimes less than one-half of the critical values). The shapes of the interaction curves may change as the pulse duration changes, and no general convexity property can be stated.

Acknowledgment

This research was supported by the National Science Foundation under Grant CME-7920781.

References

[1] Humphreys, J.S., "On Dynamic Snap Buckling of Shallow Arches," *AIAA Journal*, Vol. 4, May 1966, pp. 878-886.

[2] Fulton, R.E. and Barton, F.W., "Dynamic Buckling of Shallow Arches," *Journal of the Engineering Mechanics Division*, ASCE, Vol. 97, No. EM3, June 1971, pp. 865-877.

[3] Lock, M.H., "Snapping of a Shallow Sinusoidal Arch Under a Step Pressure Load," *AIAA Journal*, Vol. 4, July 1966, pp. 1249-1256.

[4] Hegemier, G.A. and Tzung, F., "Influence of Damping on the Snapping of a Shallow Arch Under a Step Pressure Load," *AIAA Journal*, Vol. 7, Aug. 1969, pp. 1494-1499.

[5] Huang, N.C. and Nachbar, W., "Dynamic Snap-Through of Imperfect Viscoelastic Shallow Arches," *Journal of Applied Mechanics*, Vol. 35, No. 2, June 1968, pp. 289-296.

[6] Johnson, E.R., "The Effect of Damping on Dynamic Snap-Through," *Journal of Applied Mechanics*, Vol. 47, No. 3, Sept. 1980, pp. 601-606.

[7] Gregory, W.E. Jr. and Plaut, R.H., "Dynamic Stability Boundaries for Shallow Arches," *Journal of the Engineering Mechanics Division*, ASCE, in press.

[8] Kao, R. and Perrone, N., "Dynamic Buckling of Axisymmetric Spherical Caps with Initial Imperfections," *Computers and Structures*, Vol. 9, No. 5, Nov. 1978, pp. 463-473.

[9] Budiansky, B. and Roth, R.S., "Axisymmetric Dynamic Buckling of Clamped Shallow Spherical Shells," NASA TN D-1510, Dec. 1962, pp. 597-606.

[10] Plaut, R.H. and Johnson, E.R., "The Effects of Initial Thrust and Elastic Foundation on the Vibration Frequencies of a Shallow Arch," *Journal of Sound and Vibration*, Vol. 78, No. 4, Oct. 1981, pp. 565-571.

Application of Variational Embedding Technique to Nonlinear Heat Transfer Problems

Yih-Min Chang,* Cha'o-Kuang Chen,† and Cheng-I Weng†
National Cheng Kung University
Taiwan, Republic of China

Introduction

IT is sometimes necessary to include nonlinear boundary conditions and material property variations into the analysis of a heat conduction problem.[1-5] Because these effects cannot be taken into account by using classical methods, approximate methods including these effects in a systematic manner are needed. Two such methods are the heat balance integral technique and the variational technique.

In this Note, the variational embedding technique is presented to be a new approximate method which can also include these aforesaid effects in a systematic manner. The theory of variational embedding was systematically developed by Edelem.[6] Bhatkar and Rao have applied it to the distributed systems control.[7] Now, this technique is used to solve the radiative heat transfer problem of a semi-infinite body with variable thermal properties. The results for several examples are shown in graphical form and comparisons are made with other available solutions.

Methods and Results

Consider the heat loss from a semi-infinite solid at a rate proportional to a power m of the surface temperature when both thermal conductivity and heat capacity are a function of temperature. Its initial temperature is T_0 while the ambient temperature is T_e. The governing partial differential equation for the problem can be written in the form:

$$u(T)\frac{\partial T}{\partial t} = \frac{\partial}{\partial x}\left[k(T)\frac{\partial T}{\partial x}\right] \tag{1}$$

subject to the following conditions

$$T(x,0) = T_0 \tag{2}$$

$$k\frac{\partial T}{\partial x}\bigg|_{x=0} = h[T^m(0,t) - T_e{}^m] \tag{3}$$

The thermal conductivity and heat capacity are assumed to be a power series of temperature

$$k(T) = k_R\left[1 + \sum_{j=1}^{\infty} a_j (T/T_0)^j\right] \tag{4}$$

$$u(T) = u_R\left[1 + \sum_{j=1}^{\infty} b_j (T/T_0)^j\right] \tag{5}$$

Received Oct. 9, 1981; revision received June 11, 1982.

*Researcher, Department of Mechanical Engineering.
†Professor, Department of Mechanical Engineering.

Introducing the following dimensionless parameters:

$$\theta = 1 - T/T_0, \quad \psi = 1 - [T(0,t)/T_0], \quad X = xhT_0^{m-1}/k_R$$

$$\eta = XhT_0^{m-1}/k_R, \quad \tau = (hT_0^{m-1}/k_R)^2 \alpha_R t \tag{6}$$

where $\alpha_R = k_R/u_R$ and δ is a fictitious penetration depth, Eqs. (1-3) become

$$\left[1 + \sum_{j=1}^{\infty} b_j (1-\theta)^j\right] \frac{\partial \theta}{\partial \tau} = \frac{\partial}{\partial X}\left\{\left[1 + \sum_{j=1}^{\infty} a_j (1-\theta)^j\right] \frac{\partial \theta}{\partial X}\right\} \tag{7}$$

$$\theta(X,0) = 0 \tag{8}$$

$$-\left[1 + \sum_{j=1}^{\infty} a_j (1-\theta)^j\right] \frac{\partial \theta}{\partial X} = (1-\psi)^m - u_e^m \quad \text{at} \quad X = 0 \tag{9}$$

where $u_e = T_e/T_0$.

Assume the trial function for the dimensionless temperature profile, satisfying conditions (8) and (9), to be of the form

$$\theta = \psi\left[1 - \operatorname{erf}\left(\frac{X}{\eta}\right)\right] \tag{10}$$

$$= \psi\left\{1 - \frac{2}{\sqrt{\pi}}\left[Z - \sum_{n=1}^{\infty} \frac{(-1)^{2n+1}}{n!(2n+1)} Z^{2n+1}\right]\right\} \tag{11}$$

where $Z = X/\eta$.

Choosing the adjoint function

$$\theta(X,\tau) = \frac{X}{\lambda(\tau)} \operatorname{erf}\left(\frac{x}{\eta}\right)$$

$$= \frac{2}{\sqrt{\pi}} \frac{\eta(\tau)}{\lambda(\tau)} Z^2 \left[1 - \sum_{n=1}^{\infty} \frac{(-1)^{n+1}}{n!(2n+1)} Z^{2n}\right] \tag{12}$$

the Lagrangian functional which embeds Eqs. (7-9) is

$$J[\theta,\Lambda] = \int_0^{\gamma} \int_0^{\eta(\tau)} \Lambda(X,\tau) \left\{-\left[1 + \sum_{j=1}^{\infty} b_j (1-\theta)^j\right] \frac{\partial \theta}{\partial \tau} + \frac{\partial}{\partial X}\left\{\left[1 + \sum_{j=1}^{\infty} a_j (1-\theta)^j\right] \frac{\partial \theta}{\partial X}\right\}\right\} dX d\tau \tag{13}$$

where the interval $[0,\gamma]$ is arbitrary.

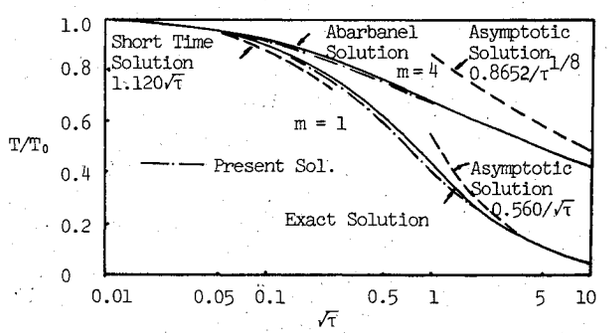

Fig. 1 Surface temperature history; heat loss from the surface of a semi-infinite solid at a rate proportional to a power m of the surface temperature.

Substituting $\theta(X,\tau)$ and $\Lambda(X,\tau)$ into Eq. (13) and integrating partially with respect to X, the Euler equation for $\lambda(\tau)$ obtained from the resulting functional comes out to be

$$\frac{d\eta^2}{d\tau}\left(M + \sum_{j=1}^{\infty} b_j N_j\right) + \sqrt{\pi}\left(P + \sum_{j=1}^{\infty} b_j Q_j\right) \frac{1}{\psi} \frac{d\psi}{d\tau} \eta^2 = 4\left(M + \sum_{j=1}^{\infty} a_j N_j\right) + \frac{4}{\sqrt{\pi}} \sum_{j=1}^{\infty} j a_j L_j \psi \tag{14}$$

where $M = 0.11015$, $P = 0.08828$

$$N_j = \int_0^1 Z^3 \left[1 - \sum_{n=1}^{\infty} \frac{(-1)^{n+1}}{n!(2n+1)} Z^{2n}\right]\left[1 - \sum_{n=1}^{\infty} \frac{(-1)^{n+1}}{n!} Z^{2n}\right] \times [1 - \psi(1 - \operatorname{erf} Z)]^j dZ$$

$$Q_j = \int_0^1 Z^2 \left[1 - \sum_{n=1}^{\infty} \frac{(-1)^{n+1}}{n!(2n+1)} Z^{2n}\right](1 - \operatorname{erf} Z) \times [1 - \psi(1 - \operatorname{erf} Z)]^j dZ$$

$$L_j = \int_0^1 Z^2 \left[1 - \sum_{n=1}^{\infty} \frac{(-1)^{n+1}}{n!(2n+1)} Z^{2n}\right]\left[1 - \sum_{n=1}^{\infty} \frac{(-1)^{n+1}}{n!} Z^{2n}\right]^2 \times [1 - \psi(1 - \operatorname{erf} Z)]^{j-1} dZ \tag{15}$$

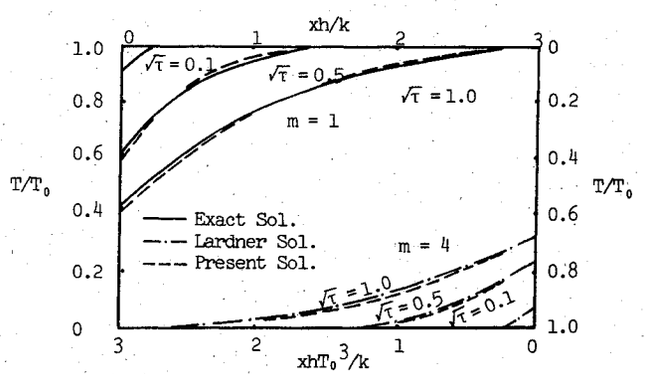

Fig. 2 Internal temperature distribution at different values of time; heat loss from the surface of a semi-infinite solid at a rate proportional to the m power of the surface temperature.

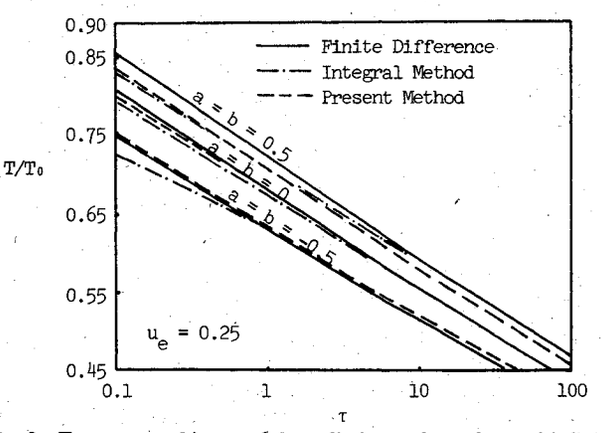

Fig. 3 Temperature history at the radiative surface of a semi-infinite solid with variable thermal properties.

From Eqs. (9) and (10), we have

$$\eta=\frac{2}{\sqrt{\pi}}\frac{\psi}{(1-\psi)^m}\left[1+\sum_{j=1}^{\infty}a_j(1-\psi)^j\right] \tag{16}$$

Substituting Eq. (16) into Eq. (14) and integrating its result, then we finally get

$$\begin{aligned}\tau=\int_0^{\psi}\Bigg\{&\left(M+\sum_{j=1}^{\infty}b_jN_j\right)2\psi\left[1+\sum_{j=1}^{\infty}a_j(1-\psi)^j\right]\\&\times\Bigg(\left[(1-\psi)^m-u_e^m\right]\left\{1+\sum_{j=1}^{\infty}a_j\left[(1-\psi)^j-j\psi(1-\psi)^{j-1}\right]\right\}\\&+m\psi\left[1+\sum_{j=1}^{\infty}a_j(1-\psi)^j\right](1-\psi)^{m-1}\Bigg)+\sqrt{\pi}\psi\left(P+\sum_{j=1}^{\infty}b_jQ_j\right)\\&\times\left[1+\sum_{j=1}^{\infty}a_j(1-\psi)^j\right]^2\left[(1-\psi)^m-u_e^m\right]\Bigg\}\\&\div\pi\left[(1-\psi)^m-u_e^m\right]^3\left(M+\sum_{j=1}^{\infty}a_jN_j+\frac{1}{\sqrt{\pi}}\sum_{j=1}^{\infty}ja_jL_j\psi\right)\mathrm{d}\psi\end{aligned} \tag{17}$$

For the case of constant thermal properties, the solution of Eq. (17) becomes

$$m=4\quad\tau=0.31831(1-\psi)^{-8}-0.57203(1-\psi)^{-7}+0.24294(1-\psi)^{-6}+0.01528 \tag{18}$$

$$m=1\quad\tau=0.31831(1-\psi)^{-2}-0.18445(1-\psi)^{-1}+0.45217\ell_n(1-\psi)-0.13386 \tag{19}$$

The surface temperature histories and internal temperature distribution which are expressed in closed analytical form are shown in Figs. 1 and 2, and compared with other available solutions.[1,2,8] The agreement is good in both cases and all of the curve no distinction between the results is evident.

In another special case, the thermal conductivity and heat capacity are assumed to be a linear function of the temperature

$$k(\theta)=1+a(1-\theta) \tag{20}$$

$$u(\theta)=1+b(1-\theta) \tag{21}$$

The solution of Eq. (17) becomes

$$\begin{aligned}\tau=\int_0^{\psi}\Bigg\{&\psi[0.22030(1+b\psi)-0.06758b\psi]\\&\times[1+a(1-\psi)]\{[(1-\psi)^m-u_e^m][1+a(1-2\psi)]\\&+m\psi[1+a(1-\psi)](1-\psi)^{m-1}\}+\psi[0.15647(1+b\psi)\\&-0.06000b\psi][1+a(1-\psi)]^2[(1-\psi)^m-u_e^m]\Bigg\}\\&\div[0.34605(1+a\psi)+0.07251a\psi][(1-\psi)^m-u_e^m]^3\mathrm{d}\psi\end{aligned} \tag{22}$$

The surface temperature histories for $m=4$; $a=+0.5$, 0, -0.5; and $b=+0.5$, 0, -0.5 are shown in Fig. 3 and compared with numerical solutions and integral solutions.[3] The agreement was found to be good. It is interesting to note that the cooling of the semi-infinite body proceeds more slowly in the case $a>0$ and $b>0$.

Remarks

For the case of material property variations, both the thermal conductivity and heat capacity can be expressed in terms of power series of variable temperature. The surface temperature history obtained by the variational embedding technique is in integral form. However, the solution becomes closed form for the constant thermal property case. The results of all considered cases have been presented in graphical form and comparisons have been made with other solutions. Agreement was found to be good. From the results of the analysis, it appears that the present technique is a simple, fast and straightforward method. In addition to the accuracy, the variational embedding technique has been shown to provide a systematic means of deducing the surface temperature history for one-dimensional nonlinear heat transfer problems.

References

[1] Abarbanel, S. S., "Time Dependent Temperature Distribution in Radiating Solids," *Journal of Mathematical Physics,* Vol. 39, 1960, pp. 246-257.

[2] Lardner, T. L., "Biot's Variational Principle in Heat Conduction," *AIAA Journal,* Vol. 1, Jan. 1961, pp. 196-206.

[3] Chung, B. T. F. and Yeh, L. T., "Analysis of Heat Transfer in Slabs with Variable Properties Subjected to Radiation and Convection," ASME Paper 75-WA/HT-67, 1975.

[4] Chambre, P. L., "Nonlinear Heat Transfer Problem," *Journal of Applied Physics,* Vol. 30, Nov. 1959, pp. 1683-1688.

[5] Crosbie, A. L. and Viskanta, R., "Transient Heating or Cooling of One-Dimensional Solids by Thermal Radiation," *Proceedings of the Third International Heat Transfer Conference*, Vol. 5, Aug. 1966, pp. 146-153.

[6] Edelem, D. G. B., *Nonlocal Variations and Local Invariance of Fields,* Elsevier, New York, 1969.

[7] Bhatkar, V. P. and Rao, B., "Variational Embedding Method and Application to Distributed Systems Control," *International Journal of Control,* Vol. 23, 1976, pp. 805-820.

[8] Carslaw, H. S. and Jaeger, J. C., *Conduction of Heat in Solids,* 2nd ed., Oxford University Press, 1959.

Evaluation of Total Body Heat Transfer in Hypersonic Flow

Richard L. Baker* and Raymond F. Kramer†
The Aerospace Corporation, El Segundo, California

Introduction

THE purpose of this Note is to provide analytic equations and calculated numerical results to enable quick and accurate evaluation of the total heat transfer to a conical body in a hypersonic flow environment. From such information, thermal protection system requirements for conical bodies in hypersonic flowfields can be determined.

Local Heat-Transfer Rates

An expression is needed for the total integrated heat transfer in hypersonic flow environments as a function of appropriate flowfield, body scale, and body geometry parameters. First, an expression is required for the local heat-transfer coefficient. In Refs. 1 and 2, the boundary-layer integral momentum equation is solved, and Reynolds analogy and a compressibility transformation are applied to obtain the

Received Dec. 21, 1981.

*Engineering Specialist, Vehicle Engineering Division.

†Manager, Reentry Applications Section, Information Processing Division.